

Bioinspiration & Biomimetics



PAPER

Stiff, strong and tough laminated glasses with bio-inspired designs

RECEIVED
17 June 2020

REVISED
21 October 2020

ACCEPTED FOR PUBLICATION
22 January 2021

PUBLISHED
15 February 2021

Zhen Yin¹  and Francois Barthelat^{1,2,*} 

¹ Department of Mechanical Engineering, McGill University, 817 Sherbrooke Street West, Montreal, QC H3A 2K6, Canada

² Department of Mechanical Engineering, University of Colorado, 427 UCB, 1111 Engineering Dr, Boulder, CO 80309, United States of America

* Author to whom any correspondence should be addressed.

E-mail: francois.barthelat@colorado.edu

Keywords: tough glass, bio-inspired, Bouligand, cross-ply, nacre-like, architected materials

Supplementary material for this article is available [online](#)

Abstract

Glass is an attractive material with outstanding transparency, hardness, durability and chemical stability. However, the inherent brittleness and low toughness of glass limit its applications. Overcoming the brittleness of glass will help satisfy the rapidly increasing demands of glass in building materials, optical devices, electronics and photovoltaic systems, but it has been a challenge to create glass that is stiff, strong and tough while maintaining its transparency. In this study we explore how the basic design of laminated glass can be enriched with bio-inspired architectures generated with laser engraving. We assess the performance of designs based on continuous plies (90° cross plies, Bouligand), finite glass blocks (segmented Bouligand, nacre-like brick-and-mortar) and hybrid designs. It shows that simultaneous improvements of stiffness, strength and energy absorption upon continuous ply designs can be achieved by promoting delocalized shearing of the polymeric interlayer over brittle fracture of the glass building blocks, and by only placing enriched architectures under tensile deformation so that interlayer shearing can be realized. This principle can be realized simply by adjusting size and arrangement of the building blocks, and by combining continuous plain layers with architected layers.

1. Introduction

Glass is a material receiving high demand in mechanical, biomedical, electronic and photovoltaic applications because of its outstanding optical properties, hardness, durability and chemical stability. However, at ambient temperature, glass is a brittle material with little deformability, leading to poor reliability and low damage tolerance in these applications [1]. Thermal or chemical tempering can increase the strength of glass by two to five-fold [2], but tempered glass suffers from catastrophic and ‘explosive’ failure by even slightest damages. Laminating glass with polymeric interlayers is another strategy that uses the interlayers to hold the glass fragments together in case of fracture which is advantageous in terms of safety, but does not change the brittleness of glass [3].

Interestingly, nature has been ‘solving’ issues associated with material brittleness for millions of years (figure 1). Many hard biological materials such as

mollusk shells and teeth are made of hard but brittle minerals, but their toughness can be thousands of times higher than their fragile constituents [4–7]. This unique combination of toughness, stiffness and strength originates from intricate material architectures at the microscopic scale [4, 8]. The microarchitectures of these biological materials generally consist of regular hard building blocks and more deformable bio-polymeric interfaces [7]. These building blocks can take a wide variety of sizes, geometries, and arrangements. For example, cross-ply structures can be found in fish scales [9–11], tooth enamel [12–14] and conch shells [15–18], formed by hard mineralized fibers or lamellae (figure 1). Cross-ply structures toughen the material by crack bridging and crack deflection. In the cuticles of many arthropod species, mineralized chitin fibers form a twisted-ply (Bouligand) structure [19, 20] (figure 1), which trigger toughening mechanisms such as crack bridging and crack twisting. Nacre from

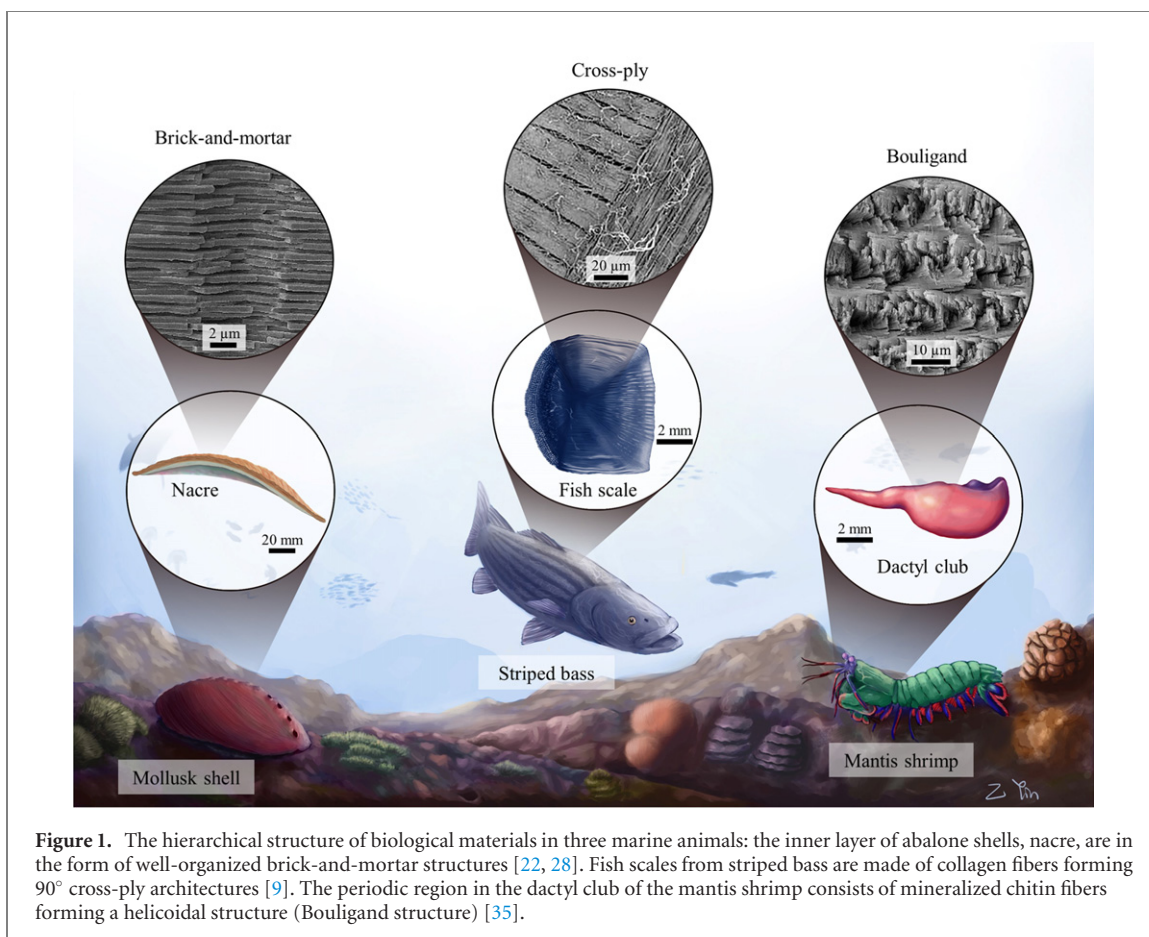


Figure 1. The hierarchical structure of biological materials in three marine animals: the inner layer of abalone shells, nacre, are in the form of well-organized brick-and-mortar structures [22, 28]. Fish scales from striped bass are made of collagen fibers forming 90° cross-ply architectures [9]. The periodic region in the dactyl club of the mantis shrimp consists of mineralized chitin fibers forming a helicoidal structure (Bouligand structure) [35].

mollusk shells has a microstructure with highly organized three-dimensional brick-and-mortar assembly of microscopic mineral tablets bonded by biopolymeric interfaces [21–23] (figure 1). These highly organized microstructures trigger delocalized toughening mechanisms such as crack deflection, crack bridging and tablet sliding that contributes to the toughness of biological materials [22]. These biological materials therefore provide interesting models as bioinspiration for toughened glasses and ceramics [24, 25].

There have been some attempts to introduce bio-inspired architectures into glass in recent years [26–29], and it has been especially challenging to achieve high combinations of hardness, stiffness, strength and toughness as well as maintaining the transparency of glass [28, 29]. A nacre-like glass was recently developed by compacting and sintering glass flakes infiltrated with refractive-index matching polymer. This material has high strength and was toughened through crack deflection [29]. However, its deformability and toughness were limited by the localized deformation, and the limited control on the microarchitectures caused decreased optical transparency due to the misalignment of the glass flakes. Other approaches include three-dimensional laser engraving to ‘carve’ interfaces and architectures within transparent glasses. For example, a nacre-inspired glass with highly controlled architectures was

developed through high precision three-dimensional laser engraving and lamination [28]. The nacre-inspired glass duplicated the large-scale tablet sliding observed in nacre, significantly outperforming plain laminated glass and tempered glass on deformability and impact resistance, but at the cost of reduced stiffness and strength [28]. Simultaneous improvement of stiffness, strength and toughness for bio-inspired architected glass remains a challenge. Bio-inspired glasses are usually based on nacre, and few studies systematically studied the effects of other material architectures and the geometry of building blocks on the mechanical performances [30]. Nacre-like, cross-ply or Bouligand structure have intricate three-dimensional architectures so that crack propagation and failure can be difficult to capture in models. Existing models for nacre-like brick-and-mortar structures have shown that toughness can be improved by promoting interlayer shearing [31, 32]. However, these models are usually in two-dimensional with simplifications. Experimental works that try to realize the simultaneous improvements for stiffness, strength and toughness of bio-inspired architected materials are still limited especially for architected laminated glass [28, 30].

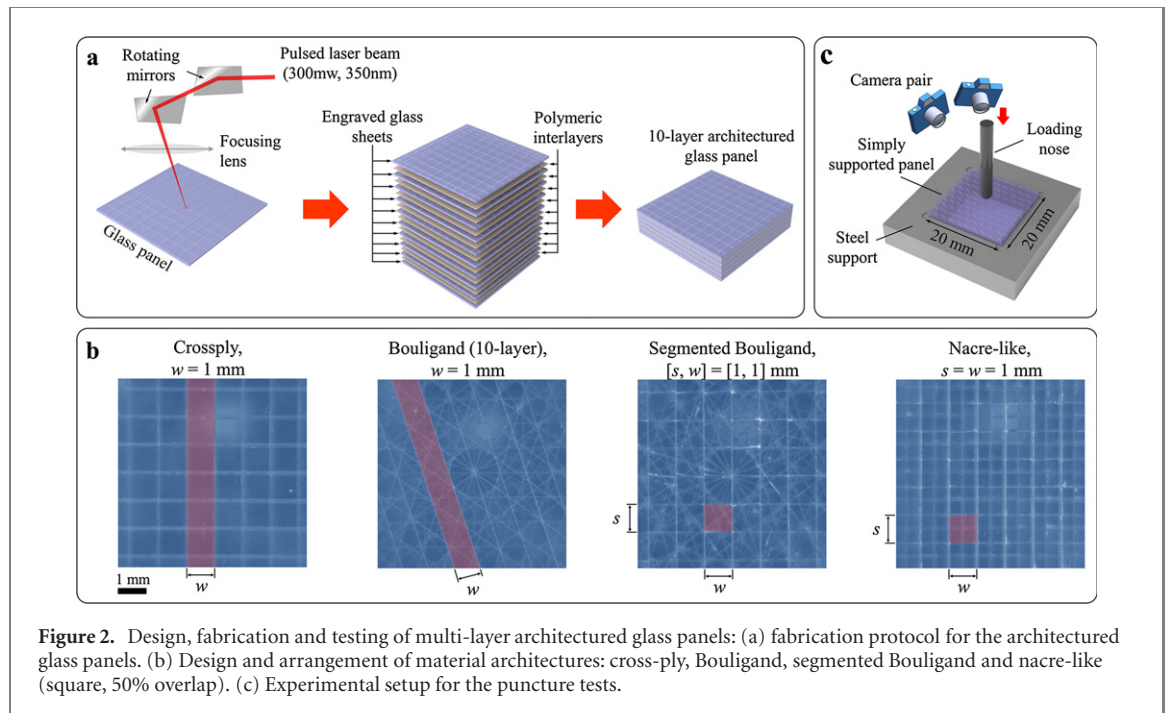
In this work, we took an experimental approach to assess and compare the mechanical performance of glass panels with various bio-inspired material architectures. General design strategies are proposed in this

paper to guide the design of stiff, strong, tough and deformable glass based on hard building blocks and ductile interlayer.

2. Design, fabrication and testing

The designs explored in this study were based on a multilayered architecture where glass layers are alternated with polymeric layers, so as to generate cross-ply, Bouligand and nacre-like architectures. We used ten 220 μm thick standard borosilicate glass sheets (20 mm \times 20 mm) (fisher scientific Hampton, NH, USA) laminated with nine 50 μm thick adhesive layers for a total laminated glass panel thickness of 2.65 mm. Ethylene-vinyl acetate (EVA) (Caida, Tianjin, China) was selected as the adhesive interface materials for its high optical transparency, strong adhesion to glass, relatively low shear strength to promote interface yielding and large inelastic deformations with energy dissipation [28]. The fraction of brittle glass in the composites are 93.1 wt%, close to the weight percent of brittle mineral contents in mollusk shells and significantly higher than other state-of-the-art bio-inspired transparent materials [29, 33]. The optical transparency of the bio-inspired glasses is comparable to the plain laminated glass under light transmittance tests (figure S1) (<http://stacks.iop.org/BB/16/026020/mmedia>). The light transmittance of bio-inspired glasses is influenced by size as well as geometric shape of the building blocks. Larger building block size allows more light to pass through the panels without the interference of the engraved interfaces. Figure 2(a) shows the general fabrication protocol. The contours of building blocks were first engraved on individual borosilicate glass sheets using a focused pulsed laser beam (300 mw) (Model Vitrolux, Vitro Laser Solutions UG, Minden, Germany). Laser engraving generates weak interfaces but keeps the integrity of glass sheets. The engraved weak interfaces were then separated mechanically after attaching polyimide films to the engraved glass sheets. The polyimide films held the building blocks in position during the mechanical separation and lamination. The engraved glass sheets were then laminated with EVA films at a temperature of 120 $^{\circ}\text{C}$ and under a uniform compression of 100 kPa. During the process, EVA infiltrated the separated engraved interfaces. The glass sheets were carefully aligned to achieve the well-controlled three-dimensional architectures considered in this study (figure 2(b)). For continuous ply designs, the patterns created within each glass layer were parallel lines to create 90 $^{\circ}$ cross-ply and Bouligand architectures (figure 2(b)). For each of these designs we considered three different ply width: $w = 1, 2$ and 3 mm. For the cross-ply architecture, the pitch angle, which is the relative ply orientation angle between two consecutive layers, was 90 $^{\circ}$ (figure 2(b)). For the Bouligand architecture, the pitch angle was

18 degree (figure 2(b)), which we chose to achieve a complete 180 degree twist of the plies through the thickness of the panel. This pitch angle is also similar to the pitch angle observed in beetle exocuticle and stomatopod dactyl club. Although pitch angle influences the mechanical responses [20, 34–36], this study fixed the pitch angle to focus on the influences of building blocks and types of architectures. In addition to Bouligand and cross-ply structures based on continuous plies, we considered segmented designs where the glass elements were squares or rectangles with finite size (width w and length s) and arranged in 3D to create segmented Bouligand and nacre-like architectures (figure 2(b)). The segmented Bouligand architecture had rectangular tablets arranged in a way similar to the continuous Bouligand architecture (figure 2(b)). The nacre-like panels had square-shape tablets with the width equaling to 1, 2 and 3 mm, staggered with a 50% overlap (figure 2(b)). We finally investigated the puncture performances of hybrid designs, where plain glass layers and architected layers were combined. The thickness of the glass sheets (Guangzhou Gking Glass, Guangzhou, China) for the plain layers was carefully selected so that the overall thickness of hybrid designs was the same as continuous ply designs and segmented designs. The glass used for the plain layers and the architected layers are of the same type with the same mechanical properties. The mechanical performance of the different architected glass panel designs was assessed using puncture tests on a simply supported configuration. The panel was placed in a custom-made steel frame to support its periphery, and a steel indenter with a 3 mm diameter spherical tip was driven through the center of the panel (figure 2(c)) at a rate of 10 $\mu\text{m s}^{-1}$ (a quasi-static loading condition) until complete puncture of the panel. A 3 mm diameter steel indenter pressed by a force of 150 N (maximum force recorded here) on a glass surface with produce an estimated contact radius of 0.15 mm (predicted from Hertz theory [37]), which is much smaller than the size of the architectures we explored here. At the same time, the indented was sufficiently blunt and the severity of the contact was not high enough to generate cracking from contact stresses: failure was dominated by flexural stresses in the panels. The test was performed using a universal test machine (model: eXpert 5000, ADMET, Norwood, MA, USA). The energy absorption capability of the panel was determined by computing the area under the force-displacement curves. Stereo-imaging was also used to monitor the deflection of the panel *in situ* (pair of synchronized cameras model IL-5, Fastec Imaging, San Diego, CA, USA). The deflection of the upper surface of the sample during puncture was reconstructed using 3D scene reconstruction methods (VIC 3D, correlated solutions, Irmo, SC, USA).

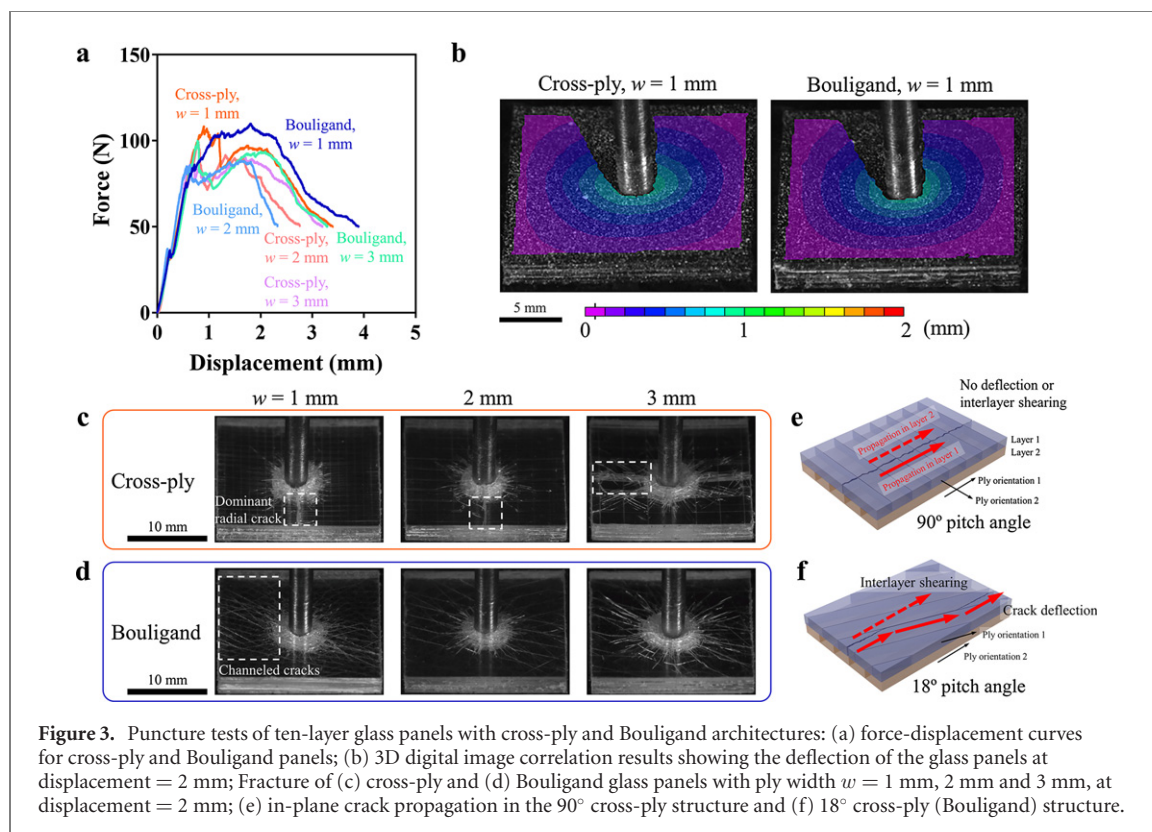


3. Continuous ply designs: 90° cross-ply and Bouligand

Figure 3(a) shows typical puncture force-displacement curves obtained from the 90° cross-ply and the Bouligand designs, with ply width $w = 1$ mm and $w = 2$ mm. In general, the curves initially showed a relatively stiff linear region, followed by a drop in force and softening associated with the fracture and sliding of individual glass plies (figure 3(a)). In all cases the failure was progressive, in contrast to plain glass where puncture failure is catastrophic and accompanied by a sharp drop in puncture force [28]. The 90° cross-ply and Bouligand panels showed similar surface deflection (figure 3(b)): the indenter punctured into the panel and heavy damages were concentrated near the puncturing site, while most of the panels have very limited deformation except for a few cracks emanating from the puncture site.

Failure occurred by brittle fracture of individual plies from flexural stresses (figures 3(c) and (d)). In the 90° cross-ply designs, radial cracks emitted from the puncture site with the longest dominant radial cracks splitting the panel in half (figures 3(c) and S2). Within some layers the dominant radial cracks propagated along the interface between adjacent plies, and in the adjacent layers the cracks propagated through the plies (the fracture of plies can be observed in figure 3(c) as the bright lines). There was no crack deflection by the interfaces between adjacent plies in a layer because of the relatively large pitch angle (figures 3(c) and (e)) [27]. For the Bouligand designs, radial cracks had a more isotropic distribution without any dominant radial cracks (figure 3(d)). These radial cracks tended to be shorter than those

in the 90° cross-ply panels (figures 3(c) and (d) and S2). For Bouligand panels with $w = 1$ mm, the in-plane cracks propagating from the puncture site were usually deflected by the interfaces between the plies within the same layer (figures 3(d) and (f)) because of the low pitch angles (18 degree). In-plane cracks channeled along the interfaces, which resulted in different crack propagation directions between neighboring layers (figure 3(f)). The difference of the crack propagation directions caused shear deformation of the polymeric interlayers that contributed to the energy absorption of the panel (figure S3) [27]. Therefore, there was no sudden force drop for the $w = 1$ mm case and the energy absorption was increased. When $w = 2$ mm and 3 mm, the panels showed more limited deformability compared to the case of $w = 1$ mm (figure 3(a)). Some of the in-plane radial cracks propagating in the glass layer were not deflected by the interfaces between the plies (figure 3(d)). Overall, continuous ply designs showed relatively limited deformability and energy absorption due to localized damage caused by the flexural stress-induced premature brittle fracture of glass plies. Decreasing the ply width could increase the deformability but the improvement was limited. Despite distinct material architectures and failure patterns, the 90° cross-ply and Bouligand panels showed generally similar stiffness, strength and energy absorption. One of the reasons for the similar performances is that premature localized fracture of plies near the puncture site occurs before deflected crack propagation can trigger and spread other toughening mechanisms such as interlayer shearing. Crack deflection alone does not contribute significantly to strength and energy absorption.

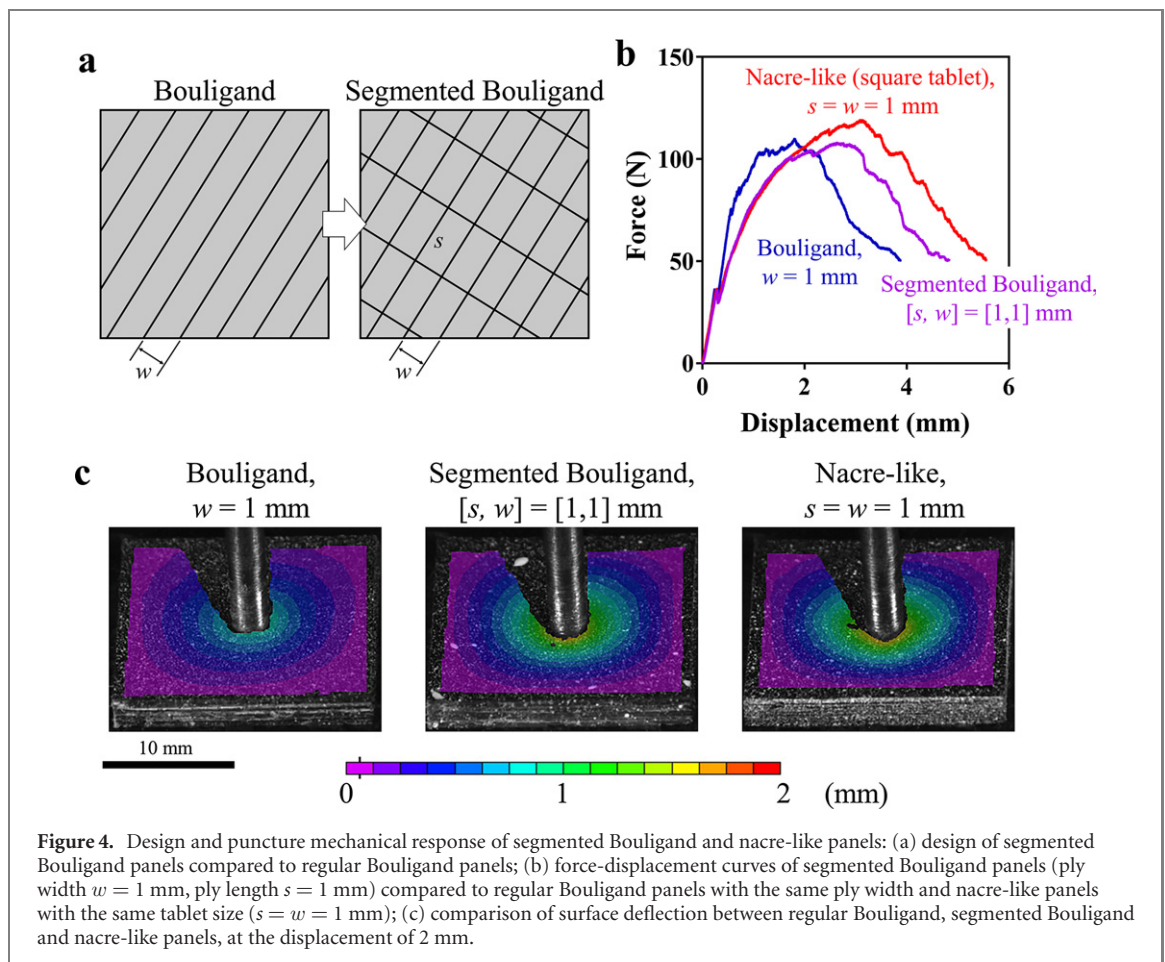


4. Segmented designs: segmented Bouligand and nacre-like panels

In both the 90° cross-ply and the Bouligand panels we observed brittle fracture of individual plies caused by flexural stresses, which led to localization and relatively limited deformability under puncture. A possible approach to better control deformation and failure in these designs is to partition the plies into segments of well-defined lengths to reduce the flexural stresses within each glass building block. We explored this route in ‘Segmented’ Bouligand designs where the plies were segmented into individual segment of length s . Another way to consider this design is that of finite glass plates of size $s \times w$ arranged in regular array within a layer, but rotated by 18° to the next layer (figure 4(a)). Another type of segmented designs we explored is the nacre-like brick-and-mortar architecture based on square tablets arranged in a staggered fashion in three dimensions. The only difference between the segmented Bouligand when $s = w$ and nacre-like panels is the arrangement of building blocks: the Bouligand architecture has a helix ply arrangement while the nacre-like is staggered (figures 1 and 2(b)).

Figure 4(b) shows typical puncture force-displacement curves for a segmented Bouligand design ($s = w = 1$ mm) and for a nacre-like design ($s = w = 1$ mm). Both designs showed an initially linear region, followed by gradual softening and an overall bell shape indicating a progressive failure.

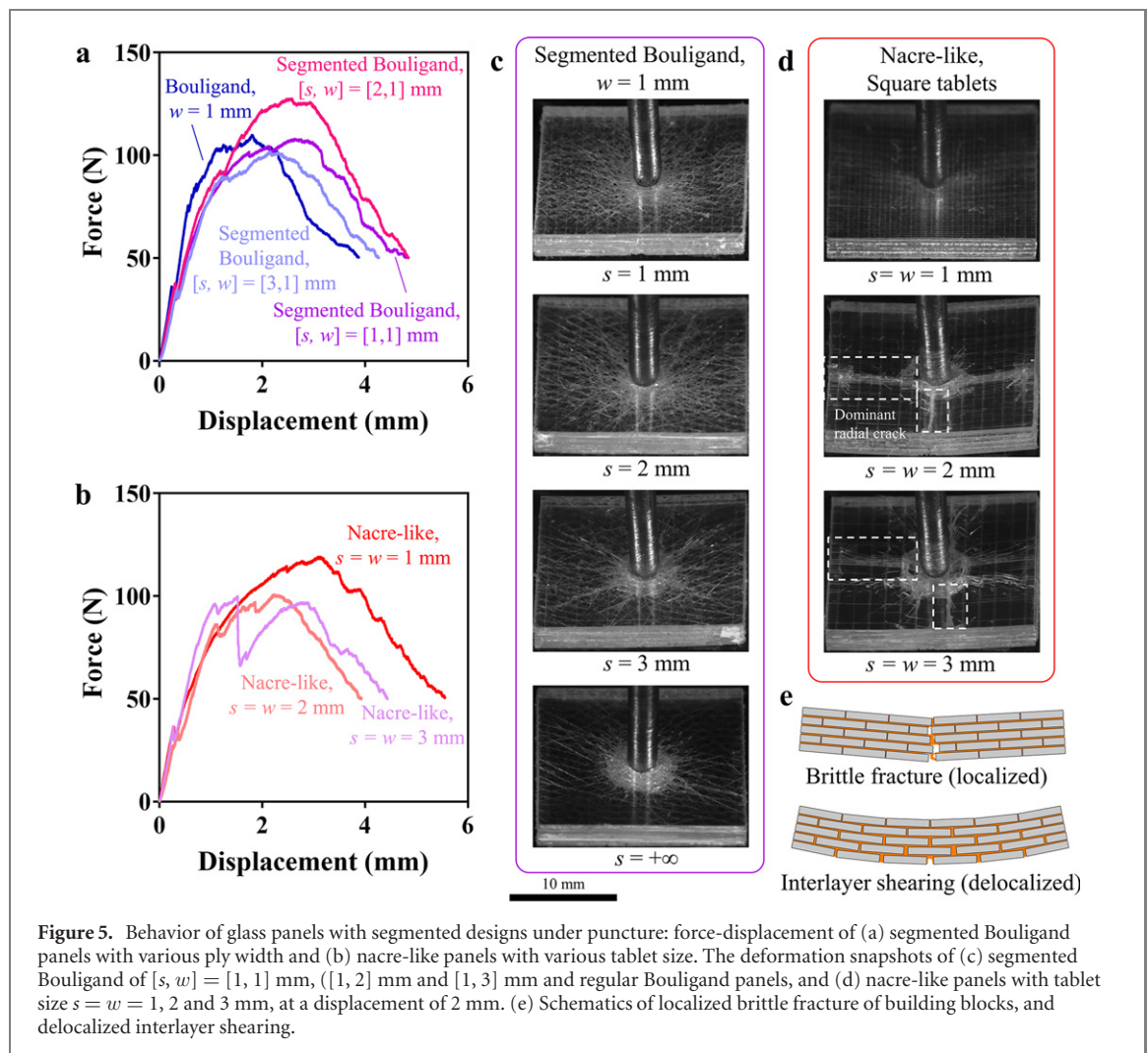
3D surface reconstructions revealed that the deformations of the segmented Bouligand and nacre-like panels were more distributed over the panel, with less abrupt ply fracture compared to the continuous designs (figure 4(c)). We varied the length of the segments using $s = 1$ mm, 2 mm and 3 mm, with a ply width kept to $w = 1$ mm (best value for continuous-ply based designs). The length of the segments had a significant impact on performance (figure 5). The segmented Bouligand panels were about 25% less stiff than the continuous ply-based panels ($s = \infty$), because the abilities of individual plies to carry stresses along their axis is reduced by the segmentation. Segmented Bouligand panels were however more deformable than the continuous design in general and significantly stronger when $[s, w] = [2, 1]$ mm. In particular, the segmented Bouligand panels with $s = 1$ mm and 2 mm were stronger and more deformable than the ones with $s = 3$ mm and $s = \infty$ (continuous plies) because localized damage was avoided by suppressed brittle fracture of building blocks, sliding between building blocks being dominant instead (figures 5(a), (c) and (e)). Interlayer shearing, resulted by the sliding between building blocks, is delocalized, which contribute to both in-plane and out-of-plane toughening. In contrast the segmented Bouligand panels with $s = 3$ mm fractured in a way similar to the regular Bouligand panels, with damage localized near the puncture site (figure 5(c)). Segmented Bouligand panels with an intermediate ply length ($s = 2$ mm) had a higher puncture strength than the panels with



$s = 1$ mm, without sacrificing deformability. We found that nacre-like panels with $s = w = 1$ mm were 15% more deformable, absorb 14% more energy and were as strong as segmented Bouligand panels ($s = 2$ mm) (figures 5(b) and 7(b)), with a better distributed deformation and damage compared to the other designs. We also observed small cracks on the top layer occurring at large displacement, which could be caused by the compressive stresses in the tablets and the shear stresses transferred from the polymeric interface [28]. Larger tablet size ($s = w = 2$ mm and $s = w = 3$ mm) led to premature brittle tablet fracture that greatly limited deformability and strength (figures 5(b) and (d)). For $s = w = 2$ mm and 3 mm, the cracks formed a cross or a ‘number sign’ (#) pattern because the in-plane crack propagation within a layer tended to follow the interfaces between the tablets. The results show that for fixed material properties of the hard and soft phases, deformation and failure modes as well as mechanical performance are very sensitive to the size of glass building blocks. Therefore, fabrication protocols with precise control on the geometry of glass building blocks are required to reach the optimal configuration of architected glass.

5. Hybrid laminated designs mixing plain and architected glass layers

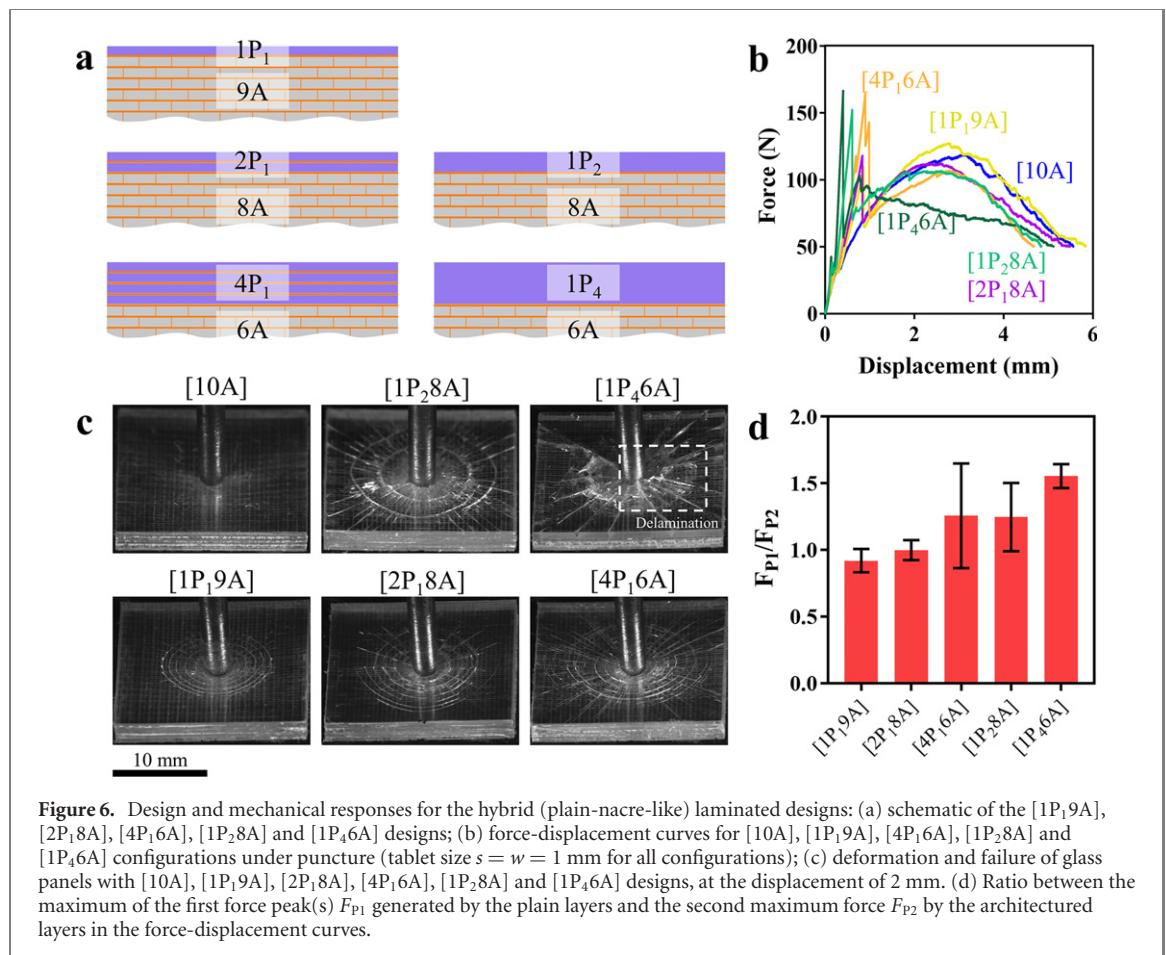
The results presented so far show how the energy absorption and deformability of multilayer architected glasses are significantly increased but at the expense of stiffness. Delocalized interlayer shearing, contributing to the high energy absorption of segmented designs, cannot be triggered when the architecture is under compressive stresses. Our previous study [28] has showed that interlayer shearing is very limited near the top surface of the panels. Therefore, a simple way to compensate for the loss in stiffness and strength is to use one or more plain, un-engraved glass layer(s) as front layer(s) where the compressive stresses are dominant. In this study we explored five configurations involving different combinations of plain and architected layers (figure 6(a)), keeping the overall thickness of the panels constant. The architected layers in all five configurations had square-shape nacre-like architecture with tablet size $s = w = 1$ mm. We used the notation $[N_p P_t N_A A]$ for each configuration, where N_p is the number of plain layers used as front layers, t is the thickness of the individual plain layers (in increments of $220 \mu\text{m}$), and N_A



is the number of architected layers. For example, [2P₁8A] is a design with two front plain layers with a thickness of $220 \mu\text{m}$ each, with eight architected layers underneath.

Figure 6(b) shows representative force-displacement curves for these hybrid designs. In general, the panels initially showed linear elastic deformation until a series of first peak(s) at a relatively high force, corresponding to the sequential failure of the plain front layer(s). Once the front layers were fractured, the underlying architected layers took over the mechanical response of the panel, producing large deformation and a second peak of maximum force (figure 6(b)). Radial and concentric cracks progressively developed in the plain layers as the indenter punctured in (figure 6(c)). The different hybrid designs showed distinct mechanical performances depending on the number and thickness of the plain layers. For example, results from the [1P₁9A], [2P₁8A] and [4P₁6A] designs show that increasing the number of plain layers increases stiffness (figures 6(b) and 7(a)). Results from the [1P₂8A] and [1P₄6A] designs show that increasing the thickness of the plain layer also substantially improved stiffness. In terms of puncture

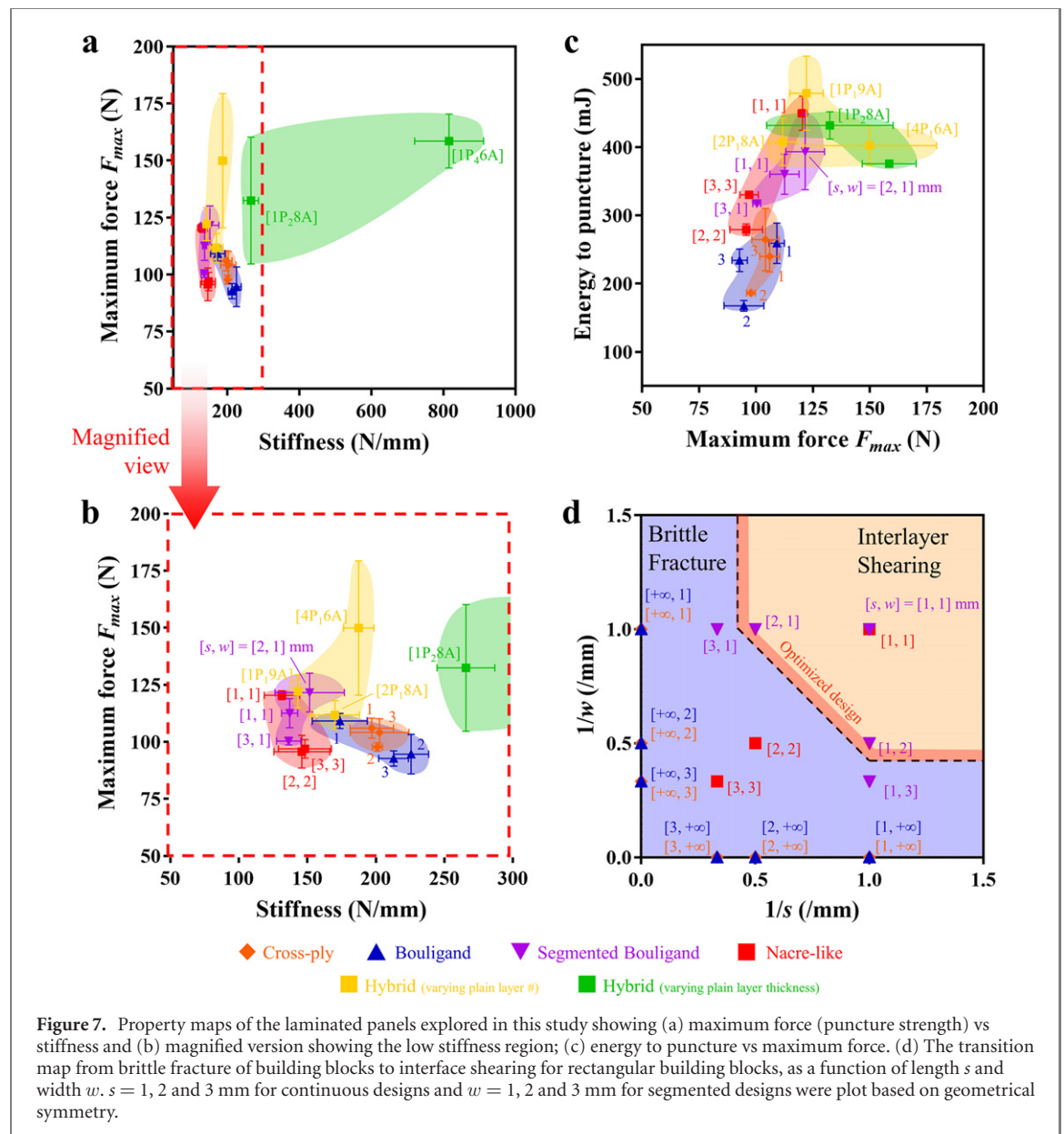
strength (maximum force), hybrid designs having with the same overall thickness of the plain layers (i.e. [4P₁6A] and [1P₄6A]) had similar maximum force. Increasing the number of plain layers (for [2P₁8A] and [4P₁6A]) and increasing the thickness of individual plain layers (for [1P₂8A] and [1P₄6A]) both improved puncture strength. The strengthening effect of the plain layers could be evaluated by the ratio between the maximum of the first peak(s) generated by the plain layers and the second more smoothly transitioned force peak generated by the architected layers (F_{P1}/F_{P2}) (figure 6(d)). For [1P₁9A], F_{P1}/F_{P2} was slightly below one, meaning that the plain layer was too thin to improve the puncture strength of the panels. Increasing the number (for [2P₁8A] and [4P₁6A]) and the thickness (for [1P₂8A] and [1P₄6A]) of the plain layer(s) could raise the F_{P1}/F_{P2} up to 1.6 (figure 6(d)), corresponding to a 60% improvement on strength. However, the strength improvement by the plain layers was not as pronounced as in our recent work ($\sim 100\%$ improvement) [28], probably due to the lower aspect ratio of the panels (width/thickness = 7.55) compared to our previous study (width/thickness = 12.5). In panels with smaller aspect ratios the plain layers



were not only under compressive stresses but also transverse shear stresses. In terms of deformability and energy absorption, [1P₁,9A] showed similar force-displacement curves after the failure of plain layers and overall deformability compared to [10A] (figure 6(b)). The second maximum force F_{p2} and overall deformability of [2P₁,8A], [4P₁,6A] and [1P₂,8A] were lower than [10A] and [1P₁,9A] (figure 6(b)) because of the relatively fewer architected layers to absorb energy through tablet sliding. Therefore, the energy absorption of these designs was inferior to [10A] and [1P₁,9A] (figure 7(b)). For [1P₄,6A], there was a rapid recovery of stiffness when the plain layer failed but the recovery ended shortly with the onset of the delamination between the plain layer and the architected layers (figure 6(c)). The delamination was caused by the highly mismatched stiffness between the plain layer and the architected layers in [1P₄,6A]. The propagation of the delamination resulted in a progressive softening of [1P₄,6A] panels. The energy absorption of [1P₄,6A] panels was relatively limited compared to other hybrid designs because of the early-stage softening caused by delamination (figures 6(b) and 7(c)).

6. Comparison of continuous ply, segmented and hybrid designs

The mechanical performances of the different glass panel designs explored in this study were displayed on the property maps showed on figures 7(a)–(c). Although the figure of merit depends on specific applications, the general goal is to move the materials to the upper right corner in the property maps, corresponding to simultaneous improvements in stiffness, strength and energy absorption. The stiffness, maximum force (puncture strength) and energy absorption of the 90° cross-ply and Bouligand panels were within the same range because in these designs the failure of the panels was dominated by the brittle fracture of glass plies (figures 7(a) and (c)). Bouligand panels with $w = 1$ mm had the highest strength and energy absorption but the lowest stiffness among all three groups of Bouligand panels tested (figure 7(b)), which was resulted by the more progressive failure of $w = 1$ mm (figures 3(a) and (d)). The segmented Bouligand designs in general had around 30% decreased stiffness, 14% increased puncture strength and 60% increased energy absorption



compared to regular Bouligand panels (figures 7(b) and (c)). The improvement of strength and energy absorption in the segmented design resulted from the suppression of brittle ply fracture with an adequate size of the building blocks. Both strength and energy absorption of segmented designs (segmented Bouligand and nacre-like) were maximized when the building blocks was at an optimized intermediate size (figure 7(c)). When the size of building blocks was too large, strength, deformability and energy absorption of segmented designs were reduced to a level close to the continuous ply designs because of the brittle fracture of the plies (or tablets) (figure 7(c)). The optimal configuration for deformability, strength and energy absorption should be at the critical point where the brittle fracture of building blocks is just suppressed (the dashed line in the failure mode map in figure 7(d)). In the hybrid designs, the plain layers substantially improve the stiffness of the segmented design (nacre-like, [10A], $s = w = 1$ mm) by up to

520% ([1P₄,6A]) (figures 7(a) and (b)). The hybrid designs also improved the puncture strength of the segmented design (nacre-like, [10A], $s = w = 1$ mm) by up to about 33% ([4P₁,6A] and [1P₄,6A]). However, replacing the front layers with plain layer did not improve energy absorption compared to nacre-like panels ($s = w = 1$ mm), and brittle plain layers resulted in relatively large deviations (5–10 samples tested for each configuration) on strength due to their sensitivity to defects (figure 7(a)). The results show that the most dominant factors for improving stiffness, strength and energy absorption are the competition between interlayer shearing and brittle fracture of building blocks. The general design principle for the simultaneous improvements on these mechanical properties is to approach the point where delocalized interlayer shearing just wins over brittle fracture of glass building blocks, and to design local architectures according to the local stress states. Our study further shows that this principle can be

realized simply by tailoring the size of the glass building blocks, and by using a hybrid design: the architected layers are under tension to provide energy absorption and plain layers are under compressive stresses to provide stiffness and strength, without introducing any complicated material architectures or hierarchy. Other parameters, such as interlayer thickness and pitch angle, can also influence the mechanical behaviors and performance but were not the focus of this study. Using Bouligand panels ($w = 2$ mm) as the reference, guided by the design principle, the hybrid design [1P₁9A] was the best in terms of energy absorption, improving energy absorption by 186% and puncture strength by 29% but had 40% reduction on stiffness. The stiffest and strongest design is the hybrid design [1P₄6A], improving stiffness by 261% and puncture strength by 67% while having 124% improvement on energy absorption compared to the reference design.

7. Summary

In this study we explored how the basic design of laminated glass can be enriched with bio-inspired architectures generated with laser engraving. Specifically, the puncture performance of bio-inspired architected glass panels evolving from continuous ply designs (cross-ply and Bouligand) to segmented designs (segmented Bouligand and square-tablet nacre-like) and hybrid designs (that incorporate plain front glass layers) were assessed. We conclude with two general principles to simultaneously improve stiffness, strength and energy absorption for architected glass materials: (i) promote delocalized interlayer shearing just right over brittle fracture of individual building blocks, and (ii) adapt local architected according to local stress state. We showed that substantial improvements on these mechanical properties can be achieved simply by tailoring the size of the glass building blocks and by using hybrid designs combining architected layers and plain layers. Our method provides a simple way to achieve large design spaces of architected glass adapting to a wide range of applications and indicates that novel composites with combinations of mechanical properties can be developed through utilizing bio-inspired synergies between architectures and interfaces.

Acknowledgments

This work was supported by a Strategic Grant (STPGP 479137–15) from the Natural Sciences and Engineering Research Council of Canada and by a Team Grant (191270) from the Fonds de Recherche du Québec—Nature et Technologies. ZY was partially

supported by a McGill Engineering Doctoral Award. The authors acknowledge Prof. Luc Mongeau (McGill University) software for 3D digital image correlation.

Conflict of interest

The authors declare no conflict of interest

ORCID iDs

Zhen Yin  <https://orcid.org/0000-0003-4068-5422>

Francois Barthelat  <https://orcid.org/0000-0001-8393-3612>

References

- [1] Zhong Z W, Tian Y B and Xie T G 2016 Investigation of subsurface damage of ground glass edges *Int. J. Adv. Manuf.* **87** 3261–9
- [2] Carré H and Daudeville L 1999 Load-bearing capacity of tempered structural glass *J. Eng. Mech.* **125** 914–21
- [3] Norville H S, King K W and Swofford J 1998 Behavior and strength of laminated glass *J. Eng. Mech.* **124** 46–53
- [4] Barthelat F 2015 Architected materials in engineering and biology: fabrication, structure, mechanics and performance *Int. Mater. Rev.* **60** 413–30
- [5] Fratzl P and Weinkamer R 2007 Nature's hierarchical materials *Prog. Mater. Sci.* **52** 1263–334
- [6] Meyers M A, Chen P-Y, Lin A Y-M and Seki Y 2008 Biological materials: structure and mechanical properties *Prog. Mater. Sci.* **53** 1–206
- [7] Barthelat F, Yin Z and Buehler M J 2016 Structure and mechanics of interfaces in biological materials *Nat. Rev. Mater.* **1** 16007
- [8] Wegst U G K, Bai H, Saiz E, Tomsia A P and Ritchie R O 2015 Bioinspired structural materials *Nat. Mater.* **14** 23–36
- [9] Zhu D, Ortega C F, Motamedi R, Szewciw L, Vernerey F and Barthelat F 2012 Structure and mechanical performance of a 'Modern' fish scale *Adv. Eng. Mater.* **14** B185–94
- [10] Yang W *et al* 2014 Protective role of *Arapaima gigas* fish scales: structure and mechanical behavior *Acta Biomater.* **10** 3599–614
- [11] Yang W, Gludovatz B, Zimmermann E A, Bale H A, Ritchie R O and Meyers M A 2013 Structure and fracture resistance of alligator gar (*atractosteus spatula*) armored fish scales *Acta Biomater.* **9** 5876–89
- [12] Bajaj D and Arola D 2009 Role of prism decussation on fatigue crack growth and fracture of human enamel *Acta Biomater.* **5** 3045–56
- [13] Bajaj D, Park S, Quinn G D and Arola D 2010 Fracture processes and mechanisms of crack growth resistance in human enamel *JOM* **62** 76–82
- [14] Yahyazadehfar M, Ivancik J, Majd H, An B, Zhang D and Arola D 2014 On the mechanics of fatigue and fracture in teeth *Appl. Mech. Rev.* **66** 030803
- [15] Menig R, Meyers M H, Meyers M A and Vecchio K S 2000 Quasi-static and dynamic mechanical response of *haliotis rufescens* (abalone) shells *Acta Mater.* **48** 2383–98
- [16] Kamat S, Kessler H, Ballarini R, Nassirou M and Heuer A H 2004 Fracture mechanisms of the *Strombus gigas* conch shell: II—micromechanics analyses of multiple cracking and large-scale crack bridging *Acta Mater.* **52** 2395–406
- [17] Kuhn-Spearing L T, Kessler H, Chateau E, Ballarini R, Heuer A H and Spearing S M 1996 Fracture mechanisms of the *Strombus gigas* conch shell: implications for the design of brittle laminates *J. Mater. Sci.* **31** 6583–94

- [18] Kamat S, Su X, Ballarini R and Heuer A H 2000 Structural basis for the fracture toughness of the shell of the conch *Strombus gigas* *Nature* **405** 1036–40
- [19] Weaver J C *et al* 2012 The stomatopod dactyl club: a formidable damage-tolerant biological hammer *Science* **336** 1275–80
- [20] Suksangpanya N, Yaraghi N A, Kisailus D and Zavattieri P 2017 Twisting cracks in Bouligand structures *J. Mech. Behav. Biomed. Mater.* **76** 38–57
- [21] Jackson A P, Vincent J F V and Turner R M 1988 The mechanical design of nacre *Proc. R. Soc. B* **234** 415–40
- [22] Barthelat F, Tang H, Zavattieri P D, Li C M and Espinosa H D 2007 On the mechanics of mother-of-pearl: a key feature in the material hierarchical structure *J. Mech. Phys. Solids* **55** 225–444
- [23] Wang R Z, Suo Z, Evans A G, Yao N and Aksay I A 2001 Deformation mechanisms in nacre *J. Mater. Res.* **16** 2485–93
- [24] Mayer G 2005 Rigid biological systems as models for synthetic composites *Science* **310** 1144–7
- [25] Barthelat F 2007 Biomimetics for next generation materials *Phil. Trans. R. Soc. A* **365** 2907–19
- [26] Mirkhalaf M, Dastjerdi A K and Barthelat F 2014 Overcoming the brittleness of glass through bio-inspiration and micro-architecture *Nat. Commun.* **5** 3166
- [27] Yin Z, Dastjerdi A and Barthelat F 2018 Tough and deformable glasses with bioinspired cross-ply architectures *Acta Biomater.* **75** 439–50
- [28] Yin Z, Hannard F and Barthelat F 2019 Impact resistant nacre-like transparent materials *Science* **364** 1260–3
- [29] Magrini T, Bouville F, Lauria A, Le Ferrand H, Niebel T P and Studart A R 2019 Transparent and tough bulk composites inspired by nacre *Nat. Commun.* **10** 2794
- [30] Jia Z, Yu Y, Hou S and Wang L 2019 Biomimetic architected materials with improved dynamic performance *J. Mech. Phys. Solids* **125** 178–97
- [31] Begley M R, Philips N R, Compton B G, Wilbrink D V, Ritchie R O and Utz M 2012 Micromechanical models to guide the development of synthetic ‘brick and mortar’ composites *J. Mech. Phys. Solids* **60** 1545–60
- [32] Abid N, Mirkhalaf M and Barthelat F 2018 Discrete-element modeling of nacre-like materials: effects of random microstructures on strain localization and mechanical performance *J. Mech. Phys. Solids* **112** 385–402
- [33] Das P, Malho J-M, Rahimi K, Schacher F H, Wang B, Demco D E and Walther A 2015 Nacre-mimetics with synthetic nanoclays up to ultrahigh aspect ratios *Nat. Commun.* **6** 5967
- [34] Apichattrabrut T and Ravi-Chandar K 2006 Helicoidal composites *Mech. Adv. Mater.* **13** 61–76
- [35] Grunenfelder L K *et al* 2014 Bio-inspired impact-resistant composites *Acta Biomater.* **10** 3997–4008
- [36] Suksangpanya N, Yaraghi N A, Pipes R B, Kisailus D and Zavattieri P 2018 Crack twisting and toughening strategies in Bouligand architectures *Int. J. Solids Struct.* **150** 83–106
- [37] Johnson K L 1985 *Contact Mechanics* (Cambridge: Cambridge University Press)